An Enantiopure J-Aggregate of Quaterrylene Bisimides for Strong Chiroptical NIR-Response

Bernhard Mahlmeister,[a] Tim Schembri,[a] Vladimir Stepanenko,[b] Kazutaka Shoyama,[b] Matthias Stolte,[a,b] and Frank Würthner[a,b]*

[a]*Center for Nanosystems Chemistry (CNC) & Bavarian Polymer Institute (BPI), Universität Würzburg, 97074 Würzburg, Germany;* [b]*Institut für Organische Chemie, Universität Würzburg, 97074 Würzburg, Germany.*

Keywords: axial chirality, excitonic chirality, fluorescence, near infrared, rylene bisimide

ABSTRACT: Chiral polycyclic aromatic hydrocarbons can be tailored for next-generation photonic materials by carefully designing their molecular as well as supramolecular architectures. Hence, excitonic coupling can boost the chiroptical response in extended aggregates but is still challenging to achieve by pure self-assembly. Whereas most reports on these potential materials cover the UV and visible spectral range, systems in the near infrared are underdeveloped. We report a new quaterrylene bisimide derivative with a conformationally stable twisted π-backbone enabled by the sterical congestion of a fourfold *bay*-arylation. Rendering the π-subplanes accessible by small imide substituents allows for a slip-stacked chiral arrangement by kinetic self-assembly in low polarity solvents. The well dispersed solid-state aggregate reveals a sharp optical signature of strong J-type excitonic coupling in both, absorption (897 nm) as well as emission (912 nm) far in the NIR region and reaches absorption dissymmetry factors up to 1.1×10^{-2}. The structural elucidation was achieved by AFM and single-crystal X-ray analysis which we combined to derive a structural model of a fourfold stranded enantiopure superhelix. We could deduce the role of phenyl substituents not only granting stable axial chirality but also guiding the chromophore into a chiral supramolecular arrangement needed for strong excitonic chirality.

INTRODUCTION

Chiral polycyclic aromatic hydrocarbons (PAHs) are considered as promising candidates for next-generation functional materials. The scope of applications ranges from displays,[1] polarization-selective photodetectors,[2,3,4,5,6] security inks[7] or even spintronic devices[8] and exploits the molecular chirality in both absorption and emission.[9] A stable and high overall chiroptical response can be achieved on a molecular level by structural design. Rigid chromophores with extended π-scaffolds have to be transformed into a conformationally stable three-dimensional chiral geometry while maintaining the high tinctorial strengths and strong fluorescence properties of the parent PAHs.[10,11,12] The required strain and contortion can be introduced into the π-scaffold in multiple ways. Common strategies include exploiting the sterical congestion of bulky substituents,[13] fusing carbonhelicenes[14,15] or embedding non-planar elements such as five- and seven-membered rings[16,17] or incorporating hetero atoms.[18,19,20] The latter can affect the PAH electronically besides purely geometrical changes to enlarge the chiroptical response.[21,22] However, the (dimensionless) molecular dissymmetry factors g_{abs} and g_{lum} of the vast majority of small organic molecules usually remain rather low in the range of 10^{-5} to 10^{-3}.[23,14,24]

However, dissymmetry factors can be significantly improved, when tailoring small molecular systems into supramolecular architectures such as dimers[25] or extended aggregates[26] by utilizing the excitonic coupling of the self-assembled dyes.[27,28,29] The supramolecular design has to balance between both an efficient exciton coupling and a favorable chiral orientation between the chromophores.[30,31,32] By this means, *g*-factors of 10^{-2} or even above could be realized for excimer-like aggregates[33] or classical H-aggregates in both solution and solid state.[9,34] Most PAHs favor a co-facial supramolecular orientation.[35] Hence, corresponding enantiopure H-type helical systems can be designed with relative ease.[36,37] In contrast, for J-aggregates it is much more demanding to meet the geometric requirements providing excitonic chirality. Thus, there are only a few reports on enantiopure J-aggregates of cyanine and squaraine dyes with strong chiroptical response of their main optical transition.[38,39] J-type excitonic coupling with narrow absorption/emission bands as well as high fluorescence quantum yields is of particular interest when approaching the deep red or near infrared (NIR) spectral region.[40,41] Recent progress could be achieved however for J-aggregates of achiral dyes.[42,43,44,45,46,47] This research field becomes currently even more relevant regarding sensing applications in biomedical research, which highlights the desire of novel chiral J-type supramolecular materials.[48]

J-aggregates based on tetra-*bay*-substituted perylene bisimides (PBIs) are known since 2007.[49] The sterical demand of the PBI´s four aryloxy substituents introduces an axial chiral twist into the chromophore core which imparts a right- or left-handed unidirectional helicity into the self-assembled cord-like aggregates (see Figure 1).[50] The conformationally stable collinear alignment of the slip-stacked chromophores within these J-aggregate is ensured by dispersion forces of the overlapping π-surfaces and is guided by hydrogen bonds between the self-complementary imide groups (Figure 1b). By this approach, helical J-aggregates are observed even from racemic mixtures due to a preferential homochiral self-assembly.[51] However, the formation of actual enantiopure J-aggregates requires separable monomers with racemization barrier $\Delta G^{\ddagger}$ of higher than 90 kJ mol^{-1}, whilst fourfold *bay*-aryloxy PBIs only show values

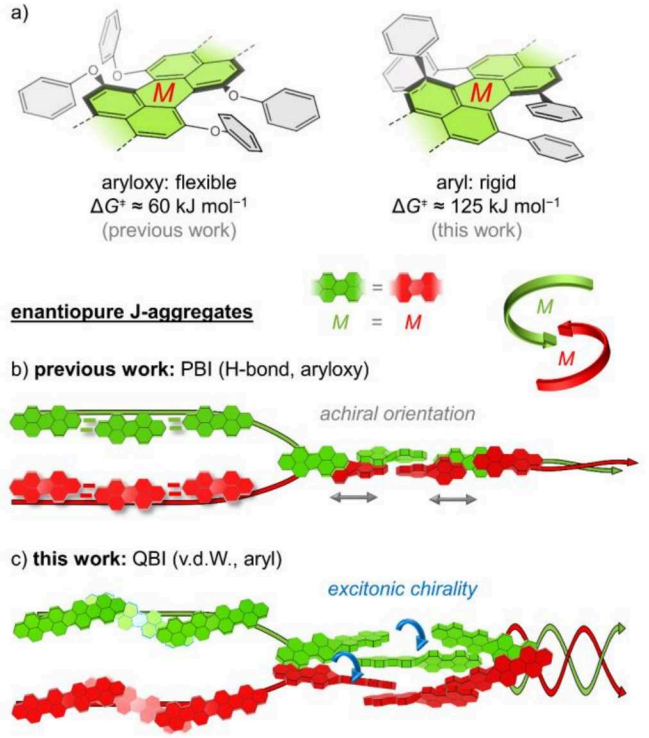

Figure 1. (a) Molecular structure of a tetra aryloxy (left) and tetraaryl (right) substituted helically twisted (*M*-) rylene core section along with their activation enthalpies for racemization. (b) Schematic depiction of H-bonded *M*-PBIs (red, green) forming a helical slip-stacked double strand with collinear (achiral) mutual orientation of the chromophores. (c) Schematic depiction of two kinked slip-stacked *M*-QBI double strands (red, green) forming an intertwined helical fourfold strand with chiral mutual orientation of the chromophores enabling excitonic chirality.

of about 60 kJ mol^{-1} at 270 K which is too low for feasible enantiomer separation.[52]

This can be synthetically realized by rigidification approaches using bridging units[53] or connecting adjacent *bay*-positions with biphenol units. By this means, the first chiral PBI J-aggregate built from stable axial chiral monomers could be realized in 2012 (Figure 1b).[54] However, due to the perfect collinear arrangement of chromophores within the aggregate, no excitonic chirality of the main J-band (absorption/emission) could be detected which would be needed to enhance the chiroptical response.

To overcome this, in the present work we follow our recent chiral interlocking approach by using directly arylated fourfold *bay*-substituted perylene cores. The corresponding *bay*-tetraarylated PBIs[55,56,13,57] have been proven to show processability as efficient non-fullerene acceptors in organic solar cells.[58,59] The sterical congestion of the aryl substituents leads to a huge twist of the PBI core (up to 39°) imparting a high conformational stability ($\Delta G^{\ddagger}$ of about 120 kJ mol^{-1} at 383 K[13]) and rigidification. In this work we could induce self-assembly of these axial-chiral molecules by expanding the π-scaffold into a core-twisted quaterrylene bisimide[60,61,62] (QBI) dye bearing only small methyl units in both imide positions. This allows self-assembly by pure van-der-Waals interactions even without H-bonding, which would facilitate an unwanted collinear (achiral) chromophore arrangement as for the *bay*-tetraaryloxy PBIs (Figure 1b). In our new work, the slip-stacked arrangement of the core-twisted enantiopure QBIs is guided into a chiral mutual orientation by the interlocking phenyl substituents[60] (see Figure 1c). This results into the formation of two intertwining slip-stacked double-strands, which wrap up into a cord-like J-aggregate with strong excitonic chirality in the NIR. To the best of our knowledge, this is unprecedented for rylene bisimide dyes so far and opens up an avenue for new supramolecular chiral materials with strong dissymmetry factors.

RESULTS AND DISCUSSION

Synthesis

The *peri*-brominated precursor **1** and the methyl-substituted naphthalimide boronic ester **2** are cross-coupled by a palladium-catalyzed 3 + 3 annulation to afford *rac*-**QBI-Me** as a racemic mixture of *P*- and *M*-atropoenantiomers (see Figure 2a, for details see the Supporting Information). The enantiomers were separated using high-performance liquid chromatography (HPLC) with a chiral stationary phase. The QBI was fully characterized by NMR, UV−Vis−NIR, and fluorescence spectroscopy as well as high-resolution mass spectrometry (Supporting Information) and X-Ray single-crystal analysis.

Optical Properties and Aggregation

First, the UV−Vis−NIR absorption properties of the racemic (*rac*) as well as *P*-/*M*-enantiopure species of **QBI-Me** were investigated in dichloromethane (DCM) solution revealing an equally strong NIR absorption of ε_{max} = 99000 M^{-1} cm^{-1} of the main S_0–S_1 transition at 800 nm (see Figure S2 (DCM) in the Supporting Information). This is in accordance to our previous report on the 2,6-diisopropylphenyl (dipp)-substituted monomeric **QBI-Dipp**.[60] However, different from **QBI-Dipp**, a distinct difference is observed by switching the solvent from DCM to very unpolar aliphatic solvents such as *n*-hexane. For **QBI-Me** with its unshielded π-surfaces, *n*-hexane is barely able to dissolve it and precipitation occurs. The racemate of **QBI-Me**

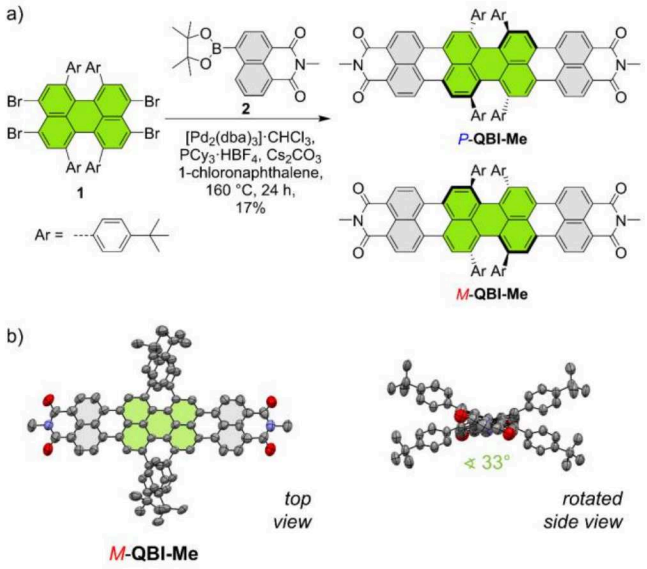

Figure 2. (a) Reaction scheme towards newly synthesized axial chiral (twisted perylene core highlighted in green) *rac*-**QBI-Me**. (b) Molecular geometry of the *M*-enantiomer found in the single-crystal structure in top view and viewed along the *N*,*N*'-axis. The ellipsoids are set to 50% probability. The twist angle between the central naphthalene subplanes is shown in green. Carbon (grey), nitrogen (blue) and oxygen (red) are indicated as well. Disordered alkyl residues and hydrogen atoms are omitted for clarity.

undergoes fast precipitation into small crystallites whereas its enantiopure *P*/*M*-species slowly forms an amorphous and well-dispersed precipitate (for details see Figure S3 in the Supporting Information). This kinetic self-assembly process was optimized for *n*-hexane by adding 2 mL of a 5 mg mL^{-1} DCM solution of *P*/*M*-**QBI-Me** into 50 mL of *n*-hexane to obtain the self-assembled species after 10 hours at 8 °C. Decantation and subsequent addition of *n*-hexane led to the disappearance of monomeric species according to the UV−Vis−NIR spectroscopy. The spectroscopic measurements of this well-dispersed aggregate of enantiopure *P*/*M*-**QBI-Me** in *n*-hexane could be conducted using transmission mode with a 1 mm cuvette after ultrasonication. In contrast, the racemic crystallites formed by fast precipitation were not suitable for measurements by this means. For comparison experiments between racemic and enantiopure species including emission data and structural investigation (vide infra) see Figures S3, S4, S8b in the Supporting Information.

To provide an appropriate monomeric reference to *P*/*M*-**QBI-Me**, a kinetically trapped monomeric *n*-hexane solution was prepared by dissolving the compound in boiling solvent and applying additional filtration using a 0.45 m PVDF syringe filter allowing measurements within a time span of one hour. The normalized UV−Vis−NIR absorption and emission spectra of this monomeric reference and the self-assembled aggregates recorded in *n*-hexane at 295 K are presented in Figure 3a and summarized in Table S1 in the Supporting Information. The monomeric reference shows its absorption maximum of the S_0–S_1 transition at 778 nm with a bandwidth (the full width at half maximum; fwhm$_{abs}$) of 810 cm^{-1} measured in *n*-hexane. The absorption maximum of the aggregated species is strongly red-shifted by 1700 cm^{-1} (119 nm) showing a pronounced NIR absorption at 897 nm. The bandwidth narrows down significantly to 530 cm^{-1} (Figure 3a) and the vibronic progression is reduced, which leads to a single sharp absorption band. Both findings are strongly indicating a J-type excitonic coupling in the aggregated state.

To probe the conversion between monomer and aggregate, we chose to track the temperature-dependent disassembly due to the kinetic nature of the self-assembly process. To guarantee an artifact-free measurement of the solid-state aggregates, spatially resolved absorption and emission measurements were conducted by using an optical microscope coupled to a spectrometer in either transmission mode on glass substrates (absorption) or reflection mode on Si/SiO$_x$ substrates (emission) upon blue light excitation (Figure 3c, and see Figure S4 in the Supporting Information for the emission study and details). The aggregate was suspended in *n*-hexane and transferred into paraffin oil onto the respective substrates to allow higher temperatures above 400 K and entailing a similar solvent polarity as *n*-hexane to preserve the spectral position of the monomeric species. Probing this disassembly at a slow heating rate of 3 K min^{-1} granted insights into the aggregation mechanism of the enantiopure *M*-**QBI-Me**. While the spatial confinement for spectral recording was kept constant during the heating process, the diffusion of molecules during disassembly could not be completely avoided. Hence, as an approximation, all spectra of the absorption study were corrected for equal total absorbance according to the Kasha exciton theory. This revealed a clear isosbestic point at 813 nm proving an equilibrium between two defined species. The degree of aggregation $\alpha = 0.85$ in paraffin oil was determined by spectral comparison with the aggregated species in *n*-hexane (see Figure 3c and Figure S4 in the Supporting Information). We then could make use of the hereby obtained temperature-dependent UV−Vis−NIR spectra at the absorption maximum of the aggregate by applying the cooperative nucleation-elongation model by Meijer, Schenning and Van der Schoot.[63] This provided an accurate fit below the elongation temperature $T_e = 389 \pm 1$ K revealing an enthalpy of

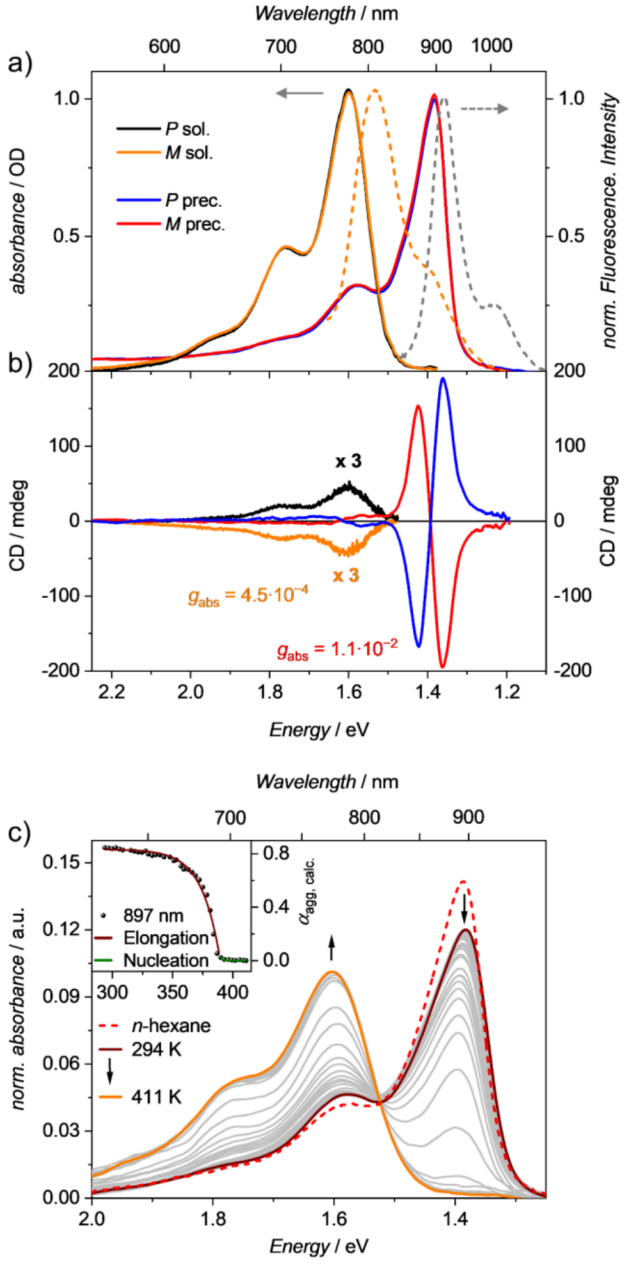

Figure 3 (a) Normalized UV−Vis−NIR absorption (solid lines) and emission (dashed lines) as well as (b) CD spectra of *P*- and *M*-**QBI-Me** in *n*-hexane at 295 K. The kinetically trapped monomeric solution (black (*P*) and orange (*M*) are scaled by a factor 3. Spectra of suspended J-aggregates are shown in blue (*P*) and red (*M*), (bottom), respectively. Absorption and emission measurements were conducted in transmission mode and front-face setup, respectively. [λ_{ex}(monomer) = 698 nm, λ_{ex}(J-aggregate) = 822 nm]. (c) UV−Vis−NIR absorption spectra for the disassembly process of *M*-**QBI-Me** in paraffin oil recorded with an optical microscope coupled into a CCD-spectrometer upon heating up to 411 K along with the reference species recorded in *n*-hexane (dashed red line). The inset shows the degree of aggregation $\alpha_{agg,calc}$ in paraffin oil at 897 nm along with the fitting curves (green, dark red) for nucleation and elongation, respectively.

$\Delta H = -83 \pm 3$ kJ/mol during the elongation process quite similar to literature known H-bonded PBI J-aggregates.[64] We were able to even estimate the equilibrium constant $K_a = 2.4 \pm 0.9 \cdot 10^{-4}$ of the activation step at T_e indicating a high degree of cooperativity reasonable for the formation of extended aggregates. We like to note that the thermally-induced disassembly occurs much faster than the racemization of the QBIs ($\Delta G^{\ddagger} \approx 125$ kJ mol^{-1} in 1,1,2,2-tetrachloroethane at 398 K[60]). Thus, the enantiopurity can be preserved after disassembly by fast heating to > 400 K (see Figure S5 in the Supporting Information).

J-aggregates have been proven to show sharp and intense emission bands, which are very desirable particularly in the NIR spectral region.[42,43,45,46,49,65] We were indeed able to observe sharp emission ($fwhm_{em} = 590$ cm^{-1}) of the suspended aggregate at 912 nm (Figure 3a). We chose a front-face setup to suppress reabsorption effects of the aggregate with its small Stokes-shift ($\Delta\tilde{\nu}_{Stokes}$) of only 180 cm^{-1}. As reference, we also recorded the emission of the monomeric *n*-hexane solution within the same sample geometry. We obtained the spectral signature of the kinetically trapped monomer revealing the maximum at 811 nm, which showed a considerably larger $\Delta\tilde{\nu}_{Stokes}$ of 520 cm^{-1} with a doubled $fwhm_{em}$ of 1080 cm^{-1} (see Table S1).

Chiroptical Properties

The high conformational stability of the axially chiral QBI monomers with a racemization barrier of about 125 kJ mol^{-1} at 398 K[60] allowed us now to investigate the transition from molecular to supramolecular chirality using circular dichroism (CD) spectroscopy. First, the monomer was investigated in DCM solution as well as in *n*-hexane as a kinetically trapped solution. Both monomeric species show a strong monosignated CD-band of their S_0-S_1 transition following the spectral progression of the respective absorption measurement with maxima at 800 nm (DCM, $\Delta\varepsilon \approx \pm 44$ M^{-1} cm^{-1}, Figure S2) and 778 nm (kinetically trapped *n*-hexane solution, $\Theta \approx 15$ mdeg at $OD = 1$, Figure 3b.) As usual for chiral PAHs, a positive sign of the lowest-energy branch of the CD spectrum corresponds to the *P*-enantiomer (and a negative sign to *M*) which is confirmed by TD-DFT calculations (*vide infra*). For these monomeric spectra, absorption dissymmetry factors g_{abs} of 4.5×10^{-4} were calculated by $g_{abs} = \varepsilon / \Delta\varepsilon$ (DCM) or $g_{abs} = \Theta/(32980 \cdot OD)$ (*n*-hexane), respectively and are within the typical range for small organic molecules.[60] However, when forming the J-aggregate in *n*-hexane, the excitonic coupling gives rise to a bisignated CD signal (couplet) maximized at 871 and 911 nm with conservative sign obeying the exciton-chirality rule. The dissymmetry factor is increased by almost two orders of magnitude to 7.0×10^{-3} (869 nm) and 1.1×10^{-2} (935 nm), respectively, while crossing zero at 903 nm close to the absorption maxima at 897 nm. To the best of our knowledge, this is the highest g_{abs} value of a chiral PAH molecule reported this far in the NIR regime. Due to strong J-type excitonic coupling, the vibrational progression is fairly suppressed, which becomes apparent around the zero-crossing of the vibrational shoulder at 767 nm.[66] Despite the high absorption dissymmetry, circularly polarized luminescence could unfortunately not be elucidated by our instrument this far in the NIR spectral range.

Structural Properties

The structural elucidation of the J-aggregate was approached by a combination of atomic force microscopy (AFM), X-ray single-crystal structure analysis and molecular modelling. For AFM measurements (Figure 4a), 60 µL of a freshly prepared aggregate suspension (500 µg of *P*/*M*/*rac*-**QBI-Me** added to 20 mL of *n*-hexane) were spin-cast onto a highly ordered pyrolytic graphite (HOPG) substrate, revealing rod-like aggregates with a length of up to 200 nm and a diameter of 2.0 ± 0.2 nm for the enantiopure *P*/*M*-species. The enantiopure aggregate structures clearly reveal a right (*P*) or left (*M*) handed helicity, each with an identical helical pitch ($p/2$) of 7.2 ± 0.6 nm. At this point we want to stress the kinetic hierarchical self-assembly. Thus, in *n*-hexane the enantiopure aggregates undergo a further aging (days to weeks) towards even more extended structures. AFM data of corresponding agglomerates reveal much more expanded rod-like structures with 12 nm diameter (see Figure S6 in the Supporting Information). The AFM of the racemate in contrast, only shows small particles with diameters of 2.9 ± 0.2 nm (Figure 4a, right, Figure S7 in the Supporting Information) with no signs of any further aging.

We related these AFM observations to the molecular arrangement within the enantiopure J-aggregate by deducing the fundamental packing geometry obtained from single-crystal X-ray diffraction (XRD) analysis of single-crystals of *rac*-**QBI-Me** grow by the slow diffusion method of methanol into a chloroform solution. Unfortunately, we could not obtain enantiopure single crystals of sufficient size and quality for XRD. *Rac*-**QBI-Me** crystallizes as a 1:1 racemic mixture in a $P\bar{1}$ space group and its unit cell contains two *P*- and *M*-atropoenantiomers, each. The molecular structure reveals a close spatial proximity of the two adjacent phenyl substituents at each side along the ribbon. These phenyl rings come as close as van-der-Waals distances of about 3.5 Å and interlock with each other entailing a rotational twist of the central part of the π-backbone (Figures 2b, 4b−e). Hence, the two inner naphthalene subplanes enclose a large dihedral angle of 33° while the outmost naphthalene subunits remain planar. This renders a large π-surface accessible to neighboring molecules to form the collinear slip-stacked geometry. By this means, two pairs of *P*- and *M*-enantiomers, top and bottom (Figure 4b), are present. The chromophores of these pairs include a 30° angle between corresponding QBI´s *N,N'*-axes and are separated by equal center-to-center distances of 14−15 Å. When forming the unit cell by superimposing both pairs, the central QBIs are in perfect collinear alignment at the same center-to-center distance (Figure 4c,d). The outer naphthalene subplanes of all QBIs within the unit cell form a fourfold stack with overall equal π-π distances of about 3.4 Å. Thus, the unit cell translates along the *cb*-axis orientation into a closely-packed slip-stacked alternating fourfold strand (Figure 4e, for an overview see Figure S9). We could indeed correlate this to the precipitated microcrystallites which were spin-cast on silicon wafers (Si/SiO_x, Figure S8a). The microcrystals of the racemate show birefringence as well as strong optical anisotropy as deduced from polarization-dependent microscopy.

Taking up this extended slip-stacked chromophore arrangement, we expected its underlying packing motif likewise for the enantiopure J-aggregates of *P*- or *M*-**QBI-Me** but with unidirectional helicity. Hence, we mimicked an enantiopure *M*-unit cell by mirroring the two *P*-enantiomers of the racemate (Figure 4d). The resulting unit cell was translated 20 times by 14.8 Å and rotated by 36° counterclockwise, each time. The resulting superhelix of 720° turn in total was then force-field optimized

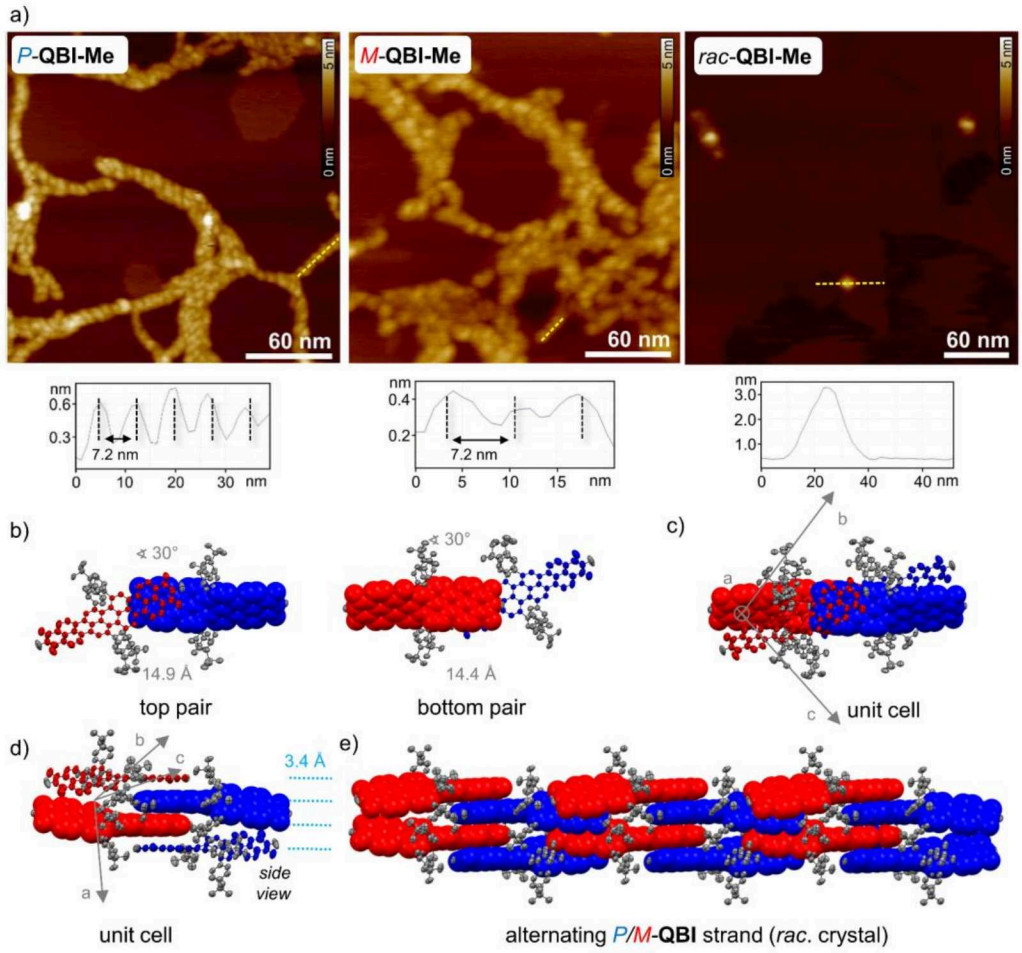

Figure 4. (a) AFM topography of self-assembled *P*- (left), *M*- (center) and *rac*- (right) **QBI-Me** after spin-casting on HOPG substrates. The insets show the cross-section analyses from yellow dashed lines in the corresponding AFM images. (b–d) Molecular arrangement of the *P*- and *M*-atropoenantiomers as determined from the single-crystal structure obtained from their racemic mixture. Two pairs (bottom and top) of next neighbored *P*- and *M*-enantiomers (blue and red) are shown in top view (b). The entire unit cell is shown in (c). The infinite translation of the unit cells is shown in side view (d). Angles between the QBI´s *N,N'*-axes and unit cell axes are shown in grey. Center-to-center distances (grey) and closest distances between π-planes (light blue) are indicated as well. The ellipsoids are set to 50% probability. Disorder, hydrogen atoms, and solvent molecules are omitted for clarity.

by using the COMPASS tool of *Materials Studio* software to eventually obtain a structural model of the J-aggregate built up from the four *M*-enantiomers A–D (Figure 5, for further details and reference computations see the Figure S10 in the Supporting Information). The measures of this optimized fourfold-stranded *M*-superhelix are in excellent agreement with the AFM parameters of the freshly prepared aggregates. They reveal a helical half pitch (*p*/2) of 7.2 nm length and a diameter of 2 nm measured between the outmost carbon atoms of the aryl *bay*-substituents within the presented model.

The whole fourfold stranded J-aggregate can be displayed in three different representations each highlighting a different dimeric packing motif of the four *M*-**QBI-Me** chromophores A–D, comprising the basic elongation unit. First, the slip-stacked chromophore pair C⇔B (Figure 5a) forms the inner core structure of the fourfold strand by showing the strongest π–π-overlap among all other QBI pairs. This pair itself is in perfect (achiral) collinear alignment but imparts the *M*-type (counterclockwise) helicity into the superstructure by the core-twist of each individual chromophore (see also Figure 1c). This supramolecular helicity now grows most prominent for the two equal slip-stacked outer pairs A⇔B and C⇔D (Figure 5b). The angles of the QBI's *N,N'*-axes of the respective pairs narrow down from 30° to 18° compared to the racemic packing (Figure 4d) and show an overall clockwise (positive, *P*) mutual orientation. The propagation of these two kinked slip-stacked pairs can be seen as two slip-stacked double strands (Figure 5b, green and red) intertwining each other in counterclockwise (*M*) sense. Already within this depiction, it becomes apparent that the QBI pairs A⇔C and B⇔D, top-stacked at double π–π-distance, are also in clockwise orientation likewise to the kinked QBIs A⇔B and C⇔D. This *P*-type handedness might be surprising but is a geometrical necessity for all *M*-intertwining double-strands that string up at small angles below 90°. Figure 5c shows these two pairs A⇔C and B⇔D in detail and highlights their π-stacked *bay*-phenyl substituents. Hence, the *P*-chiral arrangement of these superimposed QBI pairs is guided by the helical enclosing of four adjacent phenyl units. Therefore, the interlocking of the phenyl units of each chromophore not only grants stable monomeric axial chirality but ensures also the conformational stability of the overall *M*-superhelix of the J-aggregate. The elucidation of observed strong chiroptical signatures by theoretical means of all pairs of *M*-**QBI-Me** within an *M*-superhelix will be discussed in the following.

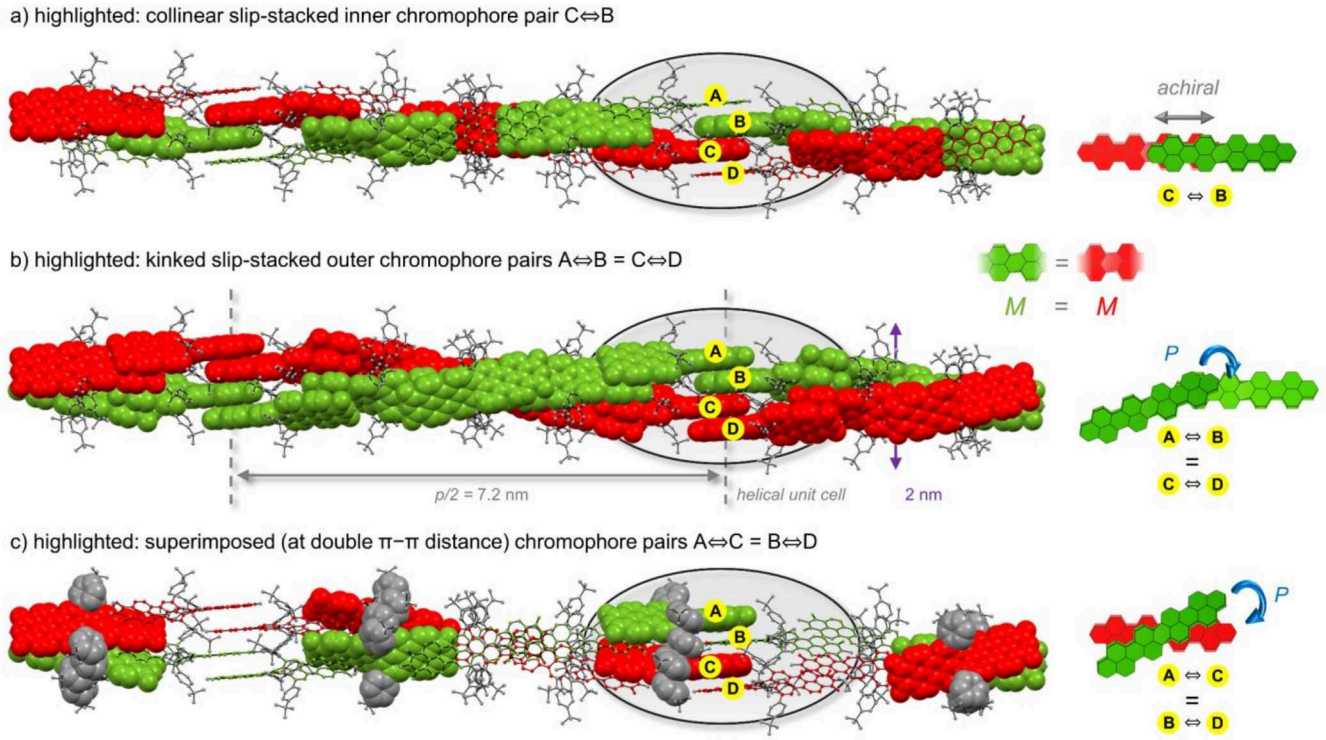

Figure 5. Structural model of the enantiopure *M*-superhelix built from ***M*-QBI-Me** chromophores derived from their molecular packing in the racemic crystal structure in three different representations (spacefill as well as ball and stick model, a–c, left) along additional schematic depictions of the corresponding pairs of QBI chromophores in top view (a–c, right). QBIs are denoted in green and red, respectively, to guide the eye to the counterclockwise *M*-type propagation of the two intertwining slip-stacked double strands (highlighted in (a,b)) forming the fourfold strand. The clockwise orientation of top-stacked chromophores within their counterclockwise intertwining double strands is highlighted in (c). The helical unit cell indicating the individual chromophores A–D (highlighted with yellow) translates into the superhelix by incremental rotating of 36°. The shown structure represents the middle section (252°) of the 720° section which was calculated in total. The structure optimization was done using the COMPASS tool of *Materials Studio* software. The helical half-pitch *p/2* (grey, calculated with centroids) and the mean distance between the outmost carbon atoms of *tert*-butyl units (violet) are indicated as well as the mutual orientation of chromophore pairs in either clockwise (*P*, blue) or collinear (*achiral*, grey) arrangement.

Theoretical calculations of chiroptical response

Electronic circular dichroism (ECD) spectra were calculated by TD-DFT on a purely electronic approach on ωB97XD/def2SVP level of theory. The obtained rotatory strength $R = \mathbf{m} \cdot \cdot \cos(\alpha)$ calculated from the magnetic (**m**) and electric ( ) transition dipole moments and their respective angle (α) is rather sensitive to the geometrical distortion imparted by the chromophore packing in the J-coupled superhelix. Thus, we re-modelled the enantiopure unit cell with geometry-optimized monomers and adapted the crucial packing parameters (see Figure S10c). The monomers were slightly simplified by replacing the *tert*-butyl units of the *bay*-substituents by hydrogen atoms. The corresponding monomeric ECD spectrum is in excellent agreement with the experiment (Figure S11 in the Supporting Information). Next, the pairs of *M*-QBIs C⇔B, C⇔D and C⇔A were simulated likewise (see Figure S12 in the Supporting Information for the following discussion). These ab-initio calculations provide two low energy excitations each, which can be interpreted as coupled states along their respective *R* with coupling strengths of 660 to 780 cm^{-1}. Hence, the superimposed *P*-type pair C⇔A, whose QBIs lie on top of each other, shows a bisignate ECD-spectrum with positive *R* for the low-energy branch. Its oscillator strength is mostly stored in the high-energy branch. Both would be reasonable for an H-type excitonic coupling. Besides, the kinked slip-stacked pair C⇔D ('creeper'-type[30,31]) shows a strong negative Cotton-effect even though its clockwise +18° orientation. The collinearly aligned slip-stacked dimer C⇔B shows (almost) no bisignate ECD-spectrum and only a single negative ECD-band hence correctly accounting for its achiral supramolecular orientation.

The opposite ECD signs of C⇔A and C⇔D, even though both pair's chromophores are in clockwise orientation, motivated for deeper analysis of the intermolecular coupling. Experimentally, the coupling strengths can be assessed by the maxima of the experimental CD-bands revealing a value of 500 cm^{-1}. For simulation of the excitonic coupling however, ab-initio TD-DFT calculations of multi-chromophore systems are rather unreliable (see the Supporting Information).[67,68] Thus, we determined the overall intermolecular coupling J_{total} by the combination of transition charge method accounting for long-range Coulomb-coupling as well as Amsterdam Density Functional (ADF) calculations for charge-transfer mediated short-range coupling (Figure 6a, Tables S4, S5 in the Supporting Information), as established for PBI aggregates.[69] We like to note that it is the large QBI transition dipole moment ($_{exp}$ = 11.6 D) which maintains a sufficient Coulomb-coupling even at long center-to-center distances of almost 15 Å compared to similar PBIs.[70] In total, reasonable J_{total} values of slip-stacked pairs of −807 cm^{-1} (100 meV, C⇔B) and −404 cm^{-1} (50 meV, C⇔D) as well as −258 cm^{-1} (32 meV) for the superimposing pair (C⇔A) could be obtained. All dimers show a negative J_{total} and hence suggest J-type excitonic coupling. This might be surprising for the top-stacked C⇔A but could be clearly attributed to the twisted and displaced mutual orientation of the chromophores. When C⇔A

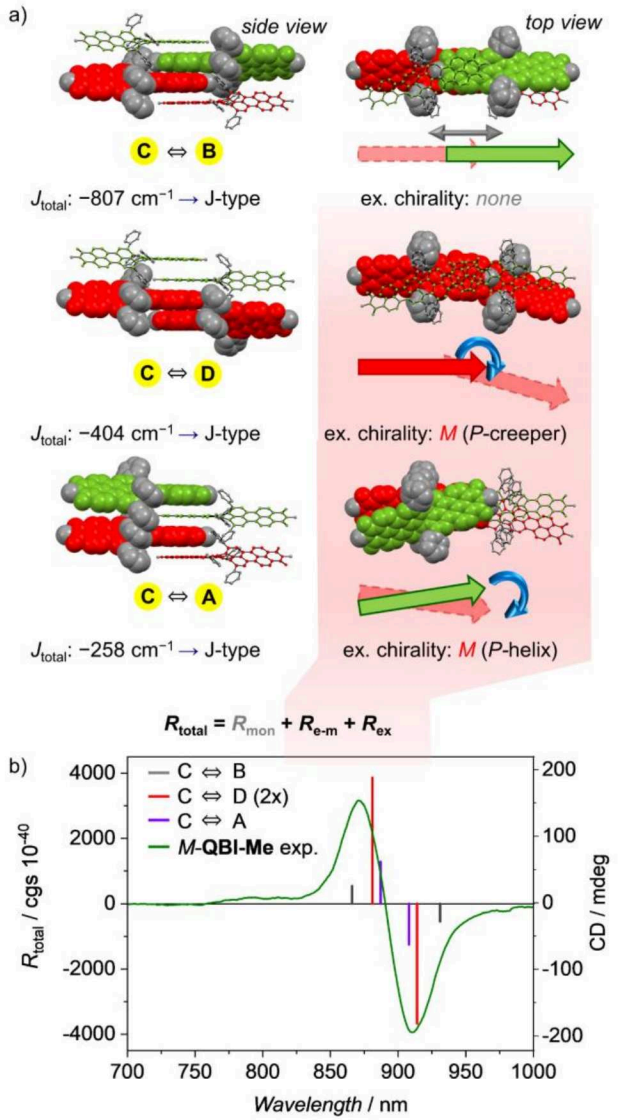

Figure 6. (a) Molecular geometries of dimers of *M*-**QBI-Me** (monomers DFT optimized) forming the core-unit of the modelled J-aggregate *M*-superhelix in side (left) and top (right) view. The arrows highlight the mutual chromophore orientation. (b) Experimental CD-spectrum (green solid line) and calculated rotatory strengths of the three dimers derived from the modified Rosenberg equation.[30] C⇔D values are doubled to adequately represent the core unit of the infinite aggregate.

is artificially parallelized into perfectly superimposing arrangement, a positive J_{total} and hence H-type coupling was obtained in corroborating reference calculations (see Figure S14, Table S6). The simulated coupling strengths now allow to interpret the mutual orientation of the chromophores. The clockwise *P*-handedness of the two chiral pairs of QBIs is indeed congruent with the common exciton chirality method[71,72] when considering their J-type coupling, which was just recently provided with theoretical understanding by Painelli, Thomas and coworkers.[30,31]

Accordingly, attractive coupling interaction leads to a negative Cotton-effect even though chromophores are in right-handed arrangement. The alleged sign-flip arises from the inversion of excitation energies of in-phase and out-of-phase combination for J- and H-type coupling, respectively. Thus, we calculated *R* of the monomers and of all dimers by applying the expanded Rosenfeld equation as sum of monomeric contribution (R_{mon}), electro-magnetic coupling ($R_{e\text{-}m}$) and excitonic contribution (R_{ex}) by using the monomeric **m** and as well as the geometric parameter from the enantiopure unit cell of the J-aggregate (Figure 6 and see the Supporting Information for details). By this means, the contribution of the superimposing pair C⇔B is restricted to R_{mon} and $R_{e\text{-}m}$ due to the perfectly collinear but achiral arrangement, while the slip-stacked pairs C⇔D and C⇔A are mostly governed by the excitonic contribution. For the low-energy branch, $R_{total\,\lambda+}$ sums up to −544 (C⇔B), −1833 (C⇔D) and -1252×10^{-40} esu^2 cm^2 (C⇔A), respectively (see Table S5). The outer kinked collinear dimer C⇔D ('creeper') is dominant due to its prominent charge-transfer coupling. Additionally, its contribution can be doubled by simple geometric considerations to account for the infinite extend of the core unit within the double strand (Figure 6b). Thus, even with this simple approach we could successfully demonstrate that the interlocking phenyl *bay*-substituents serve two functions. They ensure the conformational stability of the individual molecules and guide the QBI's self-assembly into the required handedness of the entire J-aggregate to reach strong chiroptical response in the NIR.

CONCLUSION

In summary, we presented the first enantiopure J-aggregate of a stable axial chiral rylene bisimide dye showing strong excitonic chirality of its main optical S_0–S_1 transition. A strong CD couplet centered deep in the near infrared region at 903 nm with high dissymmetry factors of up to 1.1×10^{-2} at 935 nm could be achieved. The high solubility of the tetra-arylated quaterrylene bisimide **QBI-Me** allowed for the cooperative self-assembly in low polarity *n*-hexane purely relying on weak van-der-Waals interactions enabled by the accessible large π-planes. Accordingly, we could successfully develop our concept of chiral interlocking phenyl *bay*-substituents from a molecular to a supramolecular level. Hence, the phenyl units attached to the chromophore cores not only grant conformational stability of the monomers but impart a supramolecular guiding into the helical J-aggregate. In our structural model of a slip-stacked intertwined fourfold-strand we could highlight the geometrical necessity of *P*-type handedness of close pairs of QBI chromophores to form an overall *M*-superhelix. The high photostability, spectral position in the NIR and accessibility in solid-state renders our aggregate suitable for incorporation into active host materials for chiral sensing devices.

ASSOCIATED CONTENT

Supporting Information. Supporting Information is available free of charge via the Internet at http://pubs.acs.org
Experimental and synthetic procedures, crystallographic analyses and computational details (PDF).

Accession Codes
CCDC 2252806 contains the supplementary crystallographic data for this paper. These data can be obtained free of charge via www.ccdc.cam.ac.uk/data_request/cif, or by emailing data_request@ccdc.cam.ac.uk,orby contacting The Cambridge Crystallographic Data Centre, 12 Union Road, Cambridge CB2 1EZ, UK; fax: +44 1223 336033.

Data Availability Statement. Additional data underlying this study are openly available in Zenodo at 10.5281/zenodo.7788486.

AUTHOR INFORMATION

Corresponding Author

Frank Würthner − Institut für Organische Chemie, Universität Würzburg, 97074 Würzburg, Germany; Center for Nanosystems Chemistry (CNC) & Bavarian Polymer Institute (BPI), Universität Würzburg, 97074 Würzburg, Germany; orcid.org/0000-0001-7245-0471; Email: wuerthner@uni-wuerzburg.de

Authors

Bernhard Mahlmeister − Center for Nanosystems Chemistry (CNC) & Bavarian Polymer Institute (BPI), Universität Würzburg, 97074 Würzburg, Germany

Tim Schembri − Center for Nanosystems Chemistry (CNC) & Bavarian Polymer Institute (BPI), Universität Würzburg, 97074 Würzburg, Germany

Vladimir Stepanenko − Institut für Organische Chemie, Universität Würzburg, 97074 Würzburg, Germany; orcid.org/0000-0001-7994-823X

Kazutaka Shoyama − Institut für Organische Chemie, Universität Würzburg, 97074 Würzburg, Germany; orcid.org/0000-0003-0937-4431

Matthias Stolte − Institut für Organische Chemie, Universität Würzburg, 97074 Würzburg, Germany; Center for Nanosystems Chemistry (CNC) & Bavarian Polymer Institute (BPI), Universität Würzburg, 97074 Würzburg, Germany

Contributions

All authors have given approval to the final version of the manuscript.

Notes

The authors declare no competing financial interest.

ACKNOWLEDGMENT

We acknowledge financial support from the Bavarian State Ministry for Science and the Arts for the research program "Solar Technologies Go Hybrid". The CPL/CD hybrid spectrometer was funded by the Deutsche Forschungsgemeinschaft (DFG, German Research Foundation) – Projektnummer 444286426. We acknowledge DESY (Hamburg, Germany), a member of the Helmholtz Association HGF, for providing experimental facilities at PETRA III (proposal No STP-20010322). We thank Dr. Johanna Hakanpää for assistance in using P11 beamline.

REFERENCES

(1) Deng, Y.; Wang, M.; Zhuang, Y.; Liu, S.; Huang, W.; Zhao, Q. Circularly polarized luminescence from organic micro-/nano-structures. *Light Sci. Appl.* **2021**, *10*, 76.

(2) Schulz, M.; Balzer, F.; Scheunemann, D.; Arteaga, O.; Lützen, A.; Meskers, S. C. J.; Schiek, M. Chiral Excitonic Organic Photodiodes for Direct Detection of Circular Polarized Light. *Adv. Funct. Mater.* **2019**, *29*, 1900684–1900691.

(3) Ward, M. D.; Wade, J.; Shi, X.; Nelson, J.; Campbell, A. J.; Fuchter, M. J. Highly Selective High-Speed Circularly Polarized Photodiodes Based on π-Conjugated Polymers. *Adv. Opt. Mater.* **2022**, *10*, 2101044.

(4) Zhang, L.; Song, I.; Ahn, J.; Han, M.; Linares, M.; Surin, M.; Zhang, H.-J.; Oh, J. H.; Lin, J. π-Extended perylene diimide double-heterohelicenes as ambipolar organic semiconductors for broadband circularly polarized light detection. *Nat. Commun.* **2021**, *12*, 142.

(5) Shang, X.; Song, I.; Lee, J. H.; Choi, W.; Ahn, J.; Ohtsu, H.; Kim, J. C.; Koo, J. Y.; Kwak, S. K.; Oh, J. H. Surface-Doped Quasi-2D Chiral Organic Single Crystals for Chiroptical Sensing. *ACS Nano* **2020**, *14*, 14146−14156.

(6) Song, I.; Shang, X.; Ahn, J.; Lee, J. H.; Choi, W.; Ohtsu, H.; Kim, J. C.; Kwak, S. K.; Oh, J. H. Surface Doping Effect on the Optoelectronic Properties of Tetrachloro-Substituted Chiral Perylene Diimide Supramolecular Nanowires.", *Chem. Mater.* **2022**, *34*, 8675–8683.

(7) MacKenzie, L. E.; Pal, R. Circularly polarized lanthanide luminescence for advanced security inks. *Nat. Rev. Chem.* **2021**, *5*, 109–124.

(8) Li, J.; Sanz, S.; Merino-Díez, N.; Vilas-Varela, M.; Garcia-Lekue, A.; Corso, M.; de Oteyza, Dimas G.; Frederiksen, T.; Peña, D.; Pascual, J. I. Topological phase transition in chiral graphene nanoribbons: from edge bands to end states. *Nat. Commun.* **2021**, *12*, 5538.

(9) Schulz, M.; Zablocki, J.; Abdullaeva, O. S.; Brück, S.; Balzer, F.; Lützen, A.; Artega, O.; Schiek, M. Giant intrinsic circular dichroism of prolinol-derived squaraine thin films. *Nat. Commun.* **2018**, *9*, 2413–2423.

(10) Fernández-García, J. M.; Izquierdo-García, P.; Buendía, M.; Filippone, S.; Martín, N. Synthetic chiral molecular nanographenes: the key figure of the racemization barrier. *Chem. Commun.* **2022**, *58*, 2634–2645.

(11) Ma, S.; Gu, J.; Lin, C.; Luo, Z.; Zhu, Y.; Wang, J. Supertwistacene: A Helical Graphene Nanoribbon. *J. Am. Chem. Soc.* **2020**, *142*, 16887–16893.

(12) Dubey, R. K.; Melle-Franco, M.; Mateo-Alonso, A. Inducing Single-Handed Helicity in a Twisted Molecular Nanoribbon. *J. Am. Chem. Soc.* **2022**, *144*, 2765–2774.

(13) Renner, R.; Mahlmeister, B.; Anhalt, O.; Stolte, M.; Würthner, F. Chiral Perylene Bisimide Dyes by Interlocked Arene Substituents in the Bay Area. *Chem. Eur. J.* **2021**, *27*, 11997–12006.

(14) Mori, T. Chiroptical Properties of Symmetric Double, Triple, and Multiple Helicenes. *Chem. Rev.* **2021**, *121*, 2373– 2412.

(15) Li, J.; Li, P.; Fan, M.; Zheng, X.; Guan, J.; Yin, M. Chirality of Perylene Diimides. *Angew. Chem. Int. Ed.* **2022**, *61*, e202202532.

(16) Stępień, M.; Gońka, E.; Żyła, M.; Sprutta, N. Heterocyclic Nanographenes and Other Polycyclic Heteroaromatic Compounds: Synthetic Routes, Properties, and Applications. *Chem. Rev.* **2017**, *117*, 3479−3716.

(17) Chaolumen, Stepek, I. A.; Yamada, K. E.; Ito, H.; Itami, K. Construction of Heptagon-Containing Molecular Nanocarbons. *Angew. Chem. Int. Ed.* **2021**, *60*, 23508–23532.

(18) Smith, O.; Popescu, M. V.; Hindson, M. J.; Paton, R. S.; Burton, J. W.; Smith, M. D. Control of stereogenic oxygen in a helically chiral oxonium ion. *Nature* **2023**, *615*, 430−435.

(19) Hayakawa, S.; Kawasaki, A.; Hong, Y.; Uraguchi, D.; Ooi, T.; Kim, D.; Akutagawa, T.; Fukui, N.; Shinokubo, H. Inserting Nitrogen: An Effective Concept To Create

Nonplanar and Stimuli-Responsive Perylene Bisimide Analogues *J. Am. Chem. Soc.* **2019**, *141*, 19807–19816.
(20) Liu, T.; Yang, J.; Geyer, F.; Conrad-Burton, F. S.; Sánchez, R. H.; Li, H.; Zhu, X.; Nuckolls, C.; Steigerwald, M. L., Xiao, S. Stringing the Perylene Diimide Bow. *Angew. Chem. Int. Ed.* **2020**, *59*, 14303–14307.
(21) Liu, Y.; Ma, Z.; Wang, Z.; Jiang, W. Boosting Circularly Polarized Luminescence Performance by a Double π-Helix and Heteroannulation. *J. Am. Chem. Soc.* **2022**, *144*, 11397–11404.
(22) Ma, Z.; Sun, Q.; Zhou, J.; Liu, Y.; Shuai, Z.; Wang, Z.; Jiang, W. Dual Enhancement of Emission and Luminescence Dissymmetry Factor by Si-Heteroannulation of Double π-Helix. *ACS Mater. Lett.* **2023**, *5*, 450−457.
(23) Li, X.; Yie, Y.; Li, Z. The Progress of Circularly Polarized Luminescence in Chiral Purely Organic Materials, *Adv. Photonics Res.* **2021**, *2*, 2000136.
(24) Cruz, C. M.; Castro-Fernández, S.; Maçôas, E.; Cuerva, J. M.; Campaña, A. G. Undecabenzo7superhelicene: A Helical Nanographene Ribbon as a Circularly Polarized Luminescence Emitter. *Angew. Chem. Int. Ed.* **2018**, *57*, 14782–14786.
(25) Kumar, J.; Nakashima, T.; Kawai, T. Circularly Polarized Luminescence in Chiral Molecules and Supramolecular Assemblies. *J. Phys. Chem. Lett.* **2015**, *6*, 3445–3452.
(26) Han, S. Y.; Mow, R. K.; Bartholomew, A. K.; Ng, F.; Steigerwald, M. L.; Roy, X.; Nuckolls, C.; Wiscons, R. A. Broad-band Chiral Absorbance of Visible Light. *J. Am. Chem. Soc.* **2022**, *144*, 5263−5267.
(27) Greenfield, J. L.; Wade, J.; Brandt, J. R.; Shi, X.; Penfold, T. J.; Fuchter, M. J. Pathways to increase the dissymmetry in the interaction of chiral light and chiral molecules. *Chem. Sci.* **2021**, *12*, 8589−8602.
(28) Aranda, D.; Schuster, N. J.; Xiao, X.; Ferrer, F. J. A.; Santoro, F.; Nuckolls, C. Origin of Chiroptic Amplification in Perylene-Diimide Helicenes. *J. Phys. Chem. C* **2021**, *125*, 2554−2564.
(29) Berova, N.; Di Bari, L.; Pescitelli, G. Application of electronic circular dichroism in configurational and conformational analysis of organic compounds. *Chem. Soc. Rev.* **2007**, *36*, 914–931.
(30) Swathi, K.; Sissa, C.; Painelli, A.; Thomas, K. G. Supramolecular chirality: a caveat in assigning the handedness of chiral aggregates. *Chem. Commun.* **2020**, *56*, 8281–8284.
(31) Nizar, N. S. S.; Sujith, M.; Swathi, K.; Sissa, C.; Painelli, A.; Thomas, K. G. Emergent chiroptical properties in supramolecular and plasmonic assemblies. *Chem. Soc. Rev.* **2021**, *50*, 11208–11226.
(32) Weh, M.; Rühe, J.; Herbert, B.; Krause, A.-M.; Würthner, F. Deracemization of Carbohelicenes by a Chiral Perylene Bisimide Cyclophane Template Catalyst. *Angew. Chem. Int. Ed.* **2021**, *60*, 15323–15327.
(33) Salerno, F.; Berrocal, J. A.; Haedler, A. T.; Zinna, F.; Meijer, E. W.; Di Bari, L. Highly circularly polarized broad-band emission from chiral naphthalene diimide-based supramolecular aggregates. *J. Mater. Chem. C* **2017**, *5*, 3609−3615.
(34) Mukherjee, A.; Pal, D.; Pal, D. S.; Haridas, K.; Ghosh, S. Confined supramolecular polymers in water with exceptional stability, photoluminescence and chiroptical properties. *Polym. Chem.* **2020**, *11*, 7481−7486.
(35) Würthner, F.; Saha-Möller, C. R.; Fimmel, B.; Ogi, S.; Leowanawat, P.; Schmidt, D. Perylene Bisimide Dye Assemblies as Archetype Functional Supramolecular Materials. *Chem. Rev.* **2016**, *116*, 962–1052.
(36) Wehner, M.; Röhr, M. I. S.; Bühler, M.; Stepanenko, V.; Wagner, W.; Würthner, F. Supramolecular Polymorphism in One-Dimensional Self-Assembly by Kinetic Pathway Control. *J. Am. Chem. Soc.* **2019**, *141*, 6092–6107.
(37) Wehner, M.; Röhr, M. I. S.; Stepanenko, V.; Würthner, F. Control of self-assembly pathways toward conglomerate and racemic supramolecular polymers, *Nat. Commun.* **2020**, *11*, 5460.
(38) Stoll, R. S.; Severin, N.; Rabe, J. P.; Hecht, S. Synthesis of a Novel Chiral Squaraine Dye and Its Unique Aggregation Behavior in Solution and in Self-Assembled Monolayers. *Adv. Mater.* **2006**, *18*, 1271–1275.
(39) Markova, L. I.; Malinovskii, L. V.; Patsenker, L. D.; Häner, R. J- *vs.* H-type assembly: pentamethine cyanine (Cy5) as a near-IR chiroptical reporter. *Chem. Commun.* **2013**, *49*, 5298−5300.
(40) Zampetti, A.; Minotto, A.; Cacialli, F. Near-Infrared (NIR) Organic Light-Emitting Diodes (OLEDs): Challenges and Opportunities. *Adv. Funct. Mater.* **2019**, *29*, 1807623–1807644.
(41) Meng, D.; Zheng, R.; Zhao, Y.; Zhang, E.; Dou, L.; Yang, Y. Near-Infrared Materials: The Turning Point of Organic Photovoltaics. *Adv. Mater.* **2022**, *34*, 2107330–2107356.
(42) Cai, K.; Xie, J.; Zhao, D. NIR J-Aggregates of Hydroazaheptacene Tetraimides. *J. Am. Chem. Soc.* **2014**, *136*, 28−31.
(43) Murai, M.; Abe, M.; Ogi, S.; Yamaguchi, S. Diazulenylmethyl Cations with a Silicon Bridge: A π-Extended Cationic Motif to Form J-Aggregates with Near-Infrared Absorption and Emission. *J. Am. Chem. Soc.* **2022**, *144*, 20385−20393.
(44) He, Q.; Basu, A.; Cha, H.; Daboczi, M.; Panidi, J; Tan, L.; Hu, X.; Huang, C. C.; Ding, B.; White, A. J. P.; Kim, J.-S.; Durrant, J. R.; Anthopoulos, T. D.; Heeney, M. Ultra-Narrowband Near-Infrared Responsive J-Aggregates of Fused Quinoidal Tetracyanoindacenodithiophene. *Adv. Mater.* **2023**, 2209800.
(45) Cravcenco, A.; Yu, Y.; Edhborg, F.; Goebel, J. F.; Takacs, Z.; Yang, Y.; Albinsson, B.; Börjesson, K. Exciton Delocalization Counteracts the Energy Gap: A New Pathway toward NIR-Emissive Dyes. *J. Am. Chem. Soc.* **2021**, *143*, 19232–19239.
(46) Friedman, H. C., Cosco, E. D.; Atallah, T. L.; Jia, S.; Sletten, E. M.; Caram, J. R. Establishing design principles for emissive organic SWIR chromophores from energy gap laws." *Chem* **7**(12): 3359-3376.
(47) Deshmukh, A. P.; Koppel, D.; Chuang, C.; Cadena, D. M.; Cao, J.; Caram, J. R. Design Principles for Two-Dimensional Molecular Aggregates Using Kasha's Model: Tunable Photophysics in Near and Short-Wave Infrared. *J. Phys. Chem. C* **2019**, *123*, 18702−18710.
(48) Hong, G., Antaris, A. L.; Dai, H. Near-infrared fluorophores for biomedical imaging. *Nat Biomed. Eng.* **2017**, *1*, 0010.
(49) Kaiser, T. E.; Wang, H.; Stepanenko, V.; Würthner, F. Supramolecular construction of fluorescent J-aggregates based on hydrogen-bonded perylene dyes. *Angew. Chem. Int. Ed.* **2007**, *46*, 5541–554410.

(50) Herbst, S.; Soberats, B.; Leowanawat, P.; Stolte, M.; Lehmann, M.; Würthner, F. Self-assembly of multi-stranded perylene dye J-aggregates in columnar liquid-crystalline phases. *Nat. Commun.* **2018**, *9*, 2646.

(51) Hecht, M.; Würthner, F. Supramolecularly Engineered J-Aggregates Based on Perylene Bisimide Dyes. *Acc. Chem. Res.* **2021**, *54*, 642–653.

(52) Osswald, P.; Würthner, F. Effects of Bay Substituents on the Racemization Barriers of Perylene Bisimides: Resolution of Atropo-Enantiomers. *J. Am. Chem. Soc.* **2007**, *129*, 14319–14326.

(53) Osswald, P.; Reichert, M.; Bringmann, G.; Würthner, F. Perylene Bisimide Atropisomers: Synthesis, Resolution, and Stereochemical Assignment. *J. Org. Chem.* **2007**, *72*, 3403–3411.

(54) Xie, Z.; Stepanenko, V.; Radacki, K.; Würthner, F. Chiral J-Aggregates of Atropo-Enantiomeric Perylene Bisimides and Their Self-Sorting Behavior. *Chem. Eur. J.* **2012**, *18*, 7060–7070.

(55) Qiu, W.; Chen, S.; Sun, X.; Liu, Y.; Zhu, D. Suzuki Coupling Reaction of 1,6,7,12-Tetrabromoperylene Bisimide. *Org. Lett.* **2006**, *8*, 867−870.

(56) Pagoaga, B.; Giraudet, L.; Hoffmann, N. Synthesis and Characterisation of 1,7-Di- and Inherently Chiral 1,12-Di- and 1,6,7,12-Tetraarylperylenetetracarbox-3,4:9,10-diimides. *Eur. J. Org. Chem.* **2014**, 5178−5195.

(57) Yang, W.; Longhi, G.; Abbate, S.; Lucotti, A.; Tommasini, M.; Villani, C.; Catalano, V. J.; Lykhin, A. O.; Varganov, S. A.; Chalifoux, W. A. Chiral Peropyrene: Synthesis, Structure, and Properties. *J. Am. Chem. Soc.* **2017**, *139*, 13102−13109.

(58) Cai, Y.; Huo, L.; Sun, X.; Wei, D.; Tang, M.; Sun. Y. High Performance Organic Solar Cells Based on a Twisted Bay-Substituted Tetraphenyl Functionalized Perylenediimide Electron Acceptor. *Adv. Energy Mater.* **2015**, *5*, 1500032.

(59) Mahlmeister, B.; Renner, R.; Anhalt, O.; Stolte, M.; Würthner. F. Axially chiral bay-tetraarylated perylene bisimide dyes as non-fullerene acceptors in organic solar cells. *J. Mater. Chem. C* **2022**, *10*, 2581−2591.

(60) Mahlmeister, B.; Mahl, M.; Reichelt, H.; Shoyama, K.; Stolte, M.; Würthner, F. Helically Twisted Nanoribbons Based on Emissive Near-Infrared Responsive Quaterrylene Bisimides. *J. Am. Chem. Soc.* **2022**, *144*, 10507–10514.

(61) Quante, H.; Müllen, K. Quaterrylenebis(dicarboximides). *Angew. Chem. Int. Ed.* **1995**, *34*, 1323–1325.

(62) Geerts, Y.; Quante, H.; Platz, H.; Mahrt, R.; Hopmeier, M.; Böhm, A.; Müllen, K. Quaterrylenebis(dicarboximide)s: near infrared absorbing and emitting dyes. *J. Mater. Chem.* **1998**, *8*, 2357–2369.

(63) Smulders, M. M. J.; Nieuwenhuizen, M. M. L.; de Greef, T. F. A. P.; van der Schoot, Schenning, A. P. H. J.; Meijer. E. W. How to Distinguish Isodesmic from Cooperative Supramolecular Polymerisation. *Chem. Eur. J.* **2010**, *16*, 362–367.

(64) Wagner, W.; Wehner, M.; Stepanenko, V.; Würthner, F. Supramolecular Block Copolymers by Seeded Living Polymerization of Perylene Bisimides. *J. Am. Chem. Soc.* **2019**, *141*, 12044–12054.

(65) Shen, C.-A.; Stolte, M.; Kim, J. H.; Rausch, A.; Würthner, F. Double J-Coupling Strategy for Near Infrared Emitters. *J. Am. Chem. Soc.* **2021**, *143*, 11946–11950.

(66) Spano, F. C. Analysis of the UV/Vis and CD spectral line shapes of carotenoid assemblies: spectral signatures of chiral H-aggregates. *J. Am. Chem. Soc.* **2009**, *131*, 4267–4278.

(67) Casanova-Páez, M.; Goerigk, L. Time-Dependent Long-Range-Corrected Double-Hybrid Density Functionals with Spin-Component and Spin-Opposite Scaling: A Comprehensive Analysis of Singlet–Singlet and Singlet–Triplet Excitation Energies. *J. Chem. Theory Comput.* **2020**, *17*, 5165−5186.

(68) Laidlaw, B.; Eng, J.; Wade, J.; Shi, X.; Salerno, F.; Fuchter, M. J.; Penfold, T. J. On the factors influencing the chiroptical response of conjugated polymer thin films. *Chem. Commun.* **2021**, *57*, 9914−9917.

(69) Kaufmann, C.; Bialas, D.; Stolte, M.; Würthner, F. Discrete π-Stacks of Perylene Bisimide Dyes within Folda-Dimers: Insight into Long- and Short-Range Exciton Coupling. *J. Am. Chem. Soc.* **2018**, *140*, 9986–9995.

(70) Stolte, M.; Schembri, T.; Süß, J.; Schmidt, D.; Krause, A.-M.; Vysotsky, M. O., Würthner, F. 1-Mono- and 1,7-Disubstituted Perylene Bisimide Dyes with Voluminous Groups at Bay Positions: In Search for Highly Effective Solid-State Fluorescence Materials *Chem. Mater.* **2020**, *32*, 6222–6236.

(71) Harada, N.; Chen, S.-m. L.; Nakanishi, K. Quantitative Definition of Exciton Chirality and the Distant Effect in the Exciton Chirality Method. *J. Am. Chem. Soc.* **1975**, *140*, 9986–9995.

(72) Bruhn, T.; Pescitelli, G.; Jurinovich, S.; Schaumlöffel, A.; Witterauf, F.; Ahrens, J.; Bröring, M.; Bringmann, G. Axially Chiral BODIPY DYEmers: An Apparent Exception to the Exciton Chirality Rule. *Angew. Chem. Int. Ed.* **2014**, *53*, 14592–14595.

TOC